JCSU-2401-0034 Supplementary materials

S1 Experiment

Table S1 The main element composition of X80 pipeline steel wt.%

Mn	Cr	Ni	Si	Cu	Mo	Nb
1.754	0.235	0.206	0.204	0.174	0.125	0.052
C	Al	Ti	P	V	S	Fe
0.047	0.027	0.014	0.008	0.002	0.001	Balance

Table S2 The main element composition of Zn99.995 zinc ingot wt.%

Impurities						Summation of impurities	Zn
Pb	Cd	Fe	Cu	Sn	Al		
0.003	0.002	0.001	0.001	0.001	0.001	0.005	99.995

Table S3 Composition of 1 L ATCC 1249 medium

Component	Composition	Dosage
Component I	NH_4Cl	2.0 g
	$CaSO_4$	5.0 g
	$MgSO_4$	1.0 g
	$Na_3C_6H_5O_7$ (trisodium citrate)	1.0 g
	Distilled water	400 mL
Component II	K_2HPO_4	0.5 g
	Distilled water	200 mL
Component III	$NaC_3H_5O_3$ (sodium lactate)	3.5 g
	Yeast extract	1.0 g
	Distilled water	400 mL
Component IV	Filter-sterilized 5wt% $(NH_4)_2Fe(SO_4)_2$ (ferrous ammonium sulfate). Add 20 mL of this solution to 1 L of medium prior to inoculation	

Table S4 The main chemical composition of artificial seawater g/L

NaCl	$MgSO_4 \cdot 7H_2O$	KCl	$CaCl_2 \cdot 2H_2O$	$CaCl_2 \cdot 2H_2O$	Impurity ion
21.67	5.00	4.00	1.33	1.33	0.83

Table S5 Corrosion rate of the steel after 360-h exposure in the tidal environment μm/a

Environment	HTZ	MTZ	LTZ	FIZ
SRB	397±5	353±13	249±5	69±6
SRB-CP	161±17	102±6	53±2	9±4

Table S6 Corrosion area ratio of the steel after 360-h exposure in the tidal environment %

Environment	HTZ	MTZ	LTZ	FIZ
SRB	93.0±1.1	88.4±4.4	86.2±2.1	16.7±0.4
SRB-CP	75.2±0.9	59.5±9.4	25.0±1.2	10.7±2.2

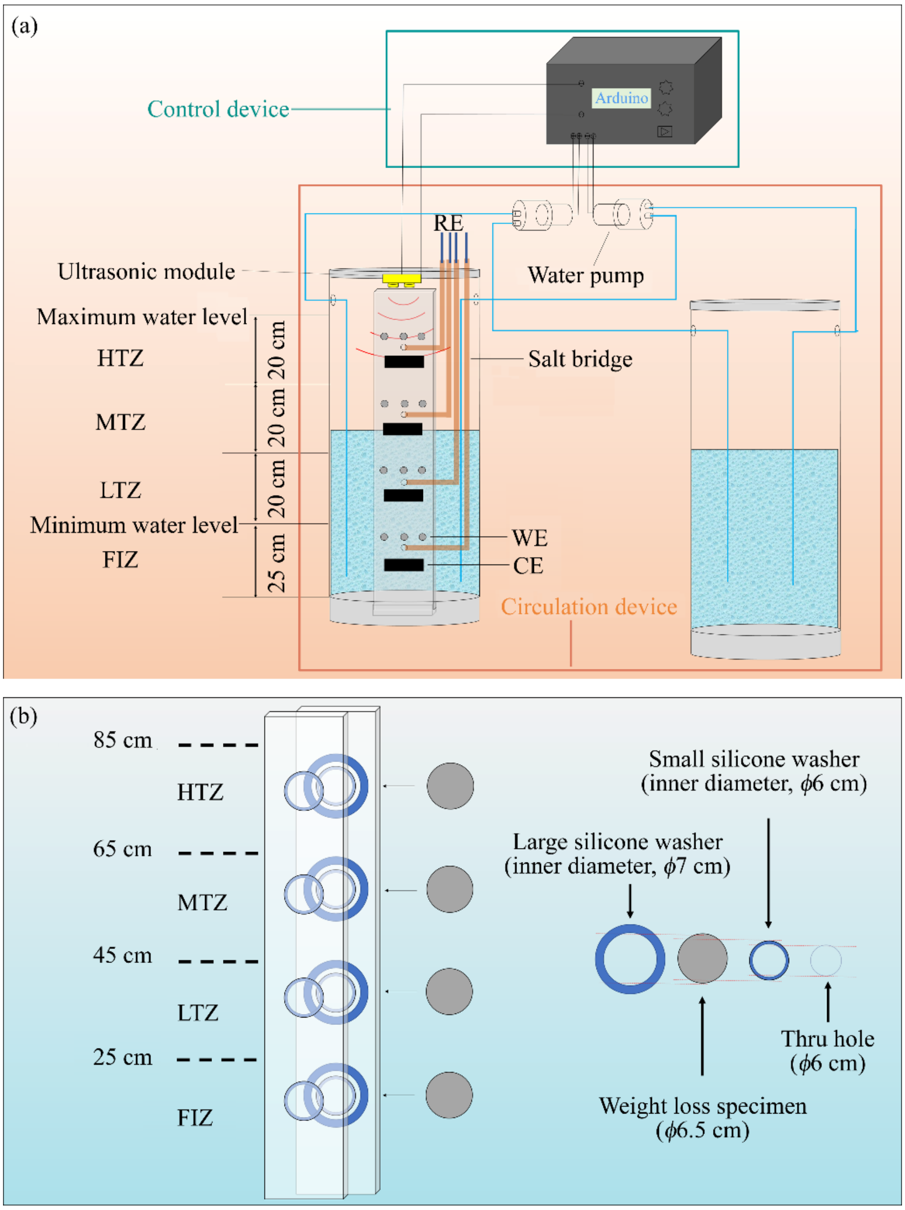

Figure S1 Schematic diagram of the tidal simulation device [2] (a), set-up of the specimens for weight loss measurements (b) (HTZ: high tidal zone; MTZ: middle tidal zone; LTZ: low tidal zone; FIZ: full immersion zone)

S1.1 Formula S1

The cathode protection potential (E_{CP}, V vs SCE) was calculated as follows [1]:

$$E_{CP} = E_{Zn} + \beta_{Zn} \ln\left(1 + \frac{A_2}{A_1}\right) \tag{S1}$$

where E_{Zn} represented the corrosion potential of Zn-SA in seawater (−1.063 vs SCE); β_{Zn} represented the andic slope of the Zn dissolution (0.06 V/dec); A_1 and A_2 represented the areas of the Zn-SA and the protected metal, respectively.

S1.2 Weight loss measurements

Before the tidal experiment, the initial weight of the specimens designated for the weight loss measurements were recorded using analytical balance ($\Delta m = 0.1$ mg). Then, the specimens were positioned in the set-up for the tidal experiment as showed in Figure S1(b), connected with the Zn-SA, and subjected to the marine tidal experiment. After the 360-h experiment, the specimens were taken out from the vessels. And the corrosion products on the specimen surfaces were removed using the rust remover consisting of 3.5 g hexamethylenetetramine, 500 mL hydrochloric acid (36 wt.%) and 500 mL deionized water. Then, the specimen surfaces were cleaned using deionized water and ethyl alcohol, and the weight of the specimens were once again recorded using the same analytical balance. Three parallel specimens were used for each group of the weight loss measurement, and the corrosion rate, *R*, of the specimen was calculated by the formula S2.

$$R=\frac{87600\times(m_0-m_1)}{\rho tA} \tag{S2}$$

where m_0 and m_1 represented the initial and final weights of the specimens, respectively; ρ and A represented the density (g/cm^3) and the total exposed area (cm^2) of the protected metals; t represented the experiment duration (h).

S1.3 Calculation of inhibition efficiency of cathode protection

The inhibition efficiency of cathode protection against the *D. desulfuricans* corrosion was determined using the formula:

$$\eta=\frac{R_1-R_2}{CR_1}\times 100\% \tag{S3}$$

where η was inhibition efficiency of cathode protection; the R_1 and R_2 were the corrosion rates of the specimens in the conditions without and with Zn-SA cathode protection, respectively.

S2 Results and analysis

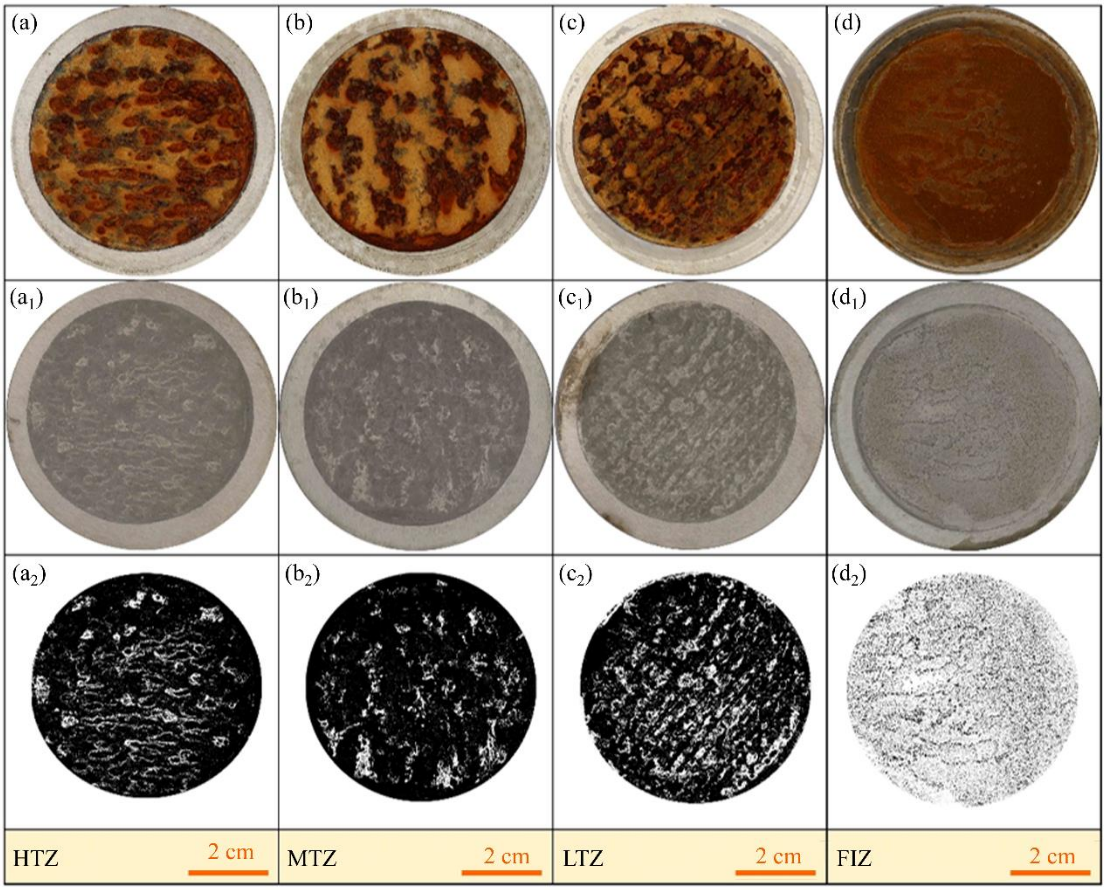

Figure S2 Macroscopic photos of the corrosion products (a–d), corrosion morphologies (a_1–d_1) and corroded area (a_2–d_2) of the steel after 360-h exposure in the biotic tidal environment without the cathode protection

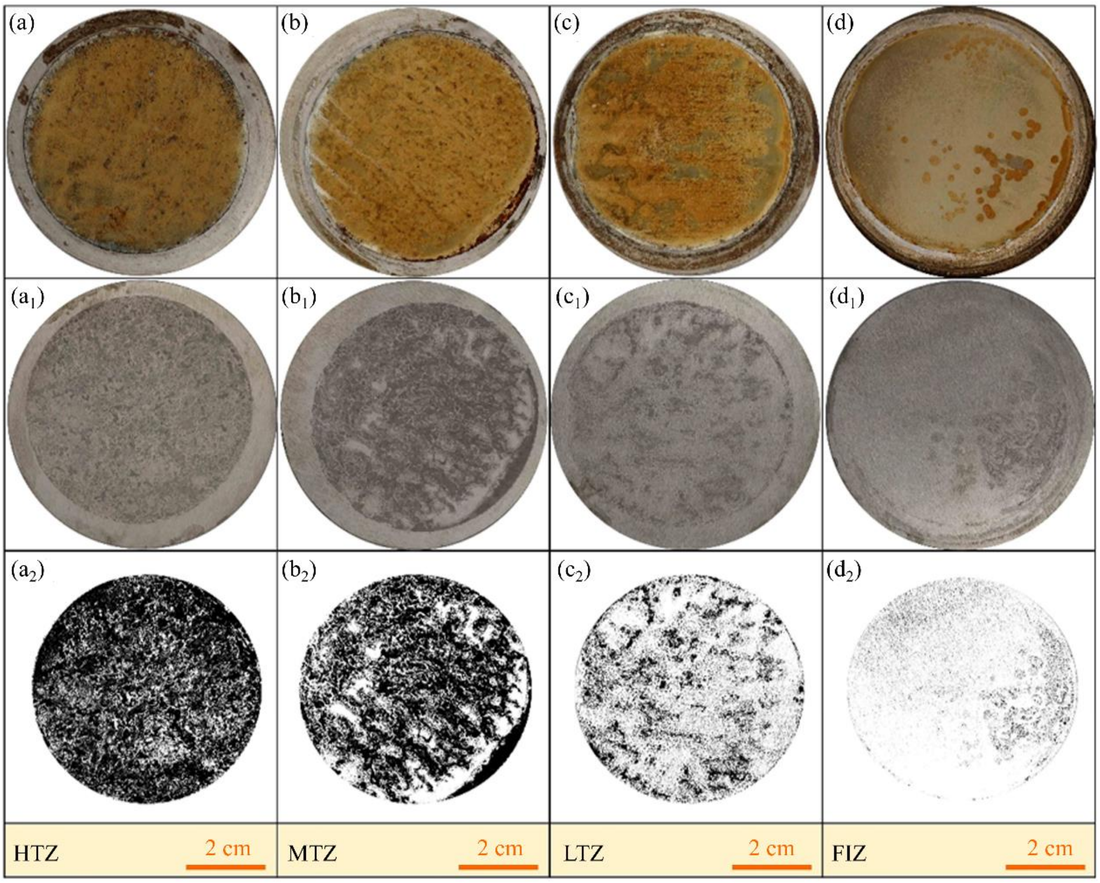

Figure S3 Macroscopic photos of the corrosion products (a–d), corrosion morphologies (a_1–d_1) and corroded area (a_2–d_2) of the steel after 360-h exposure in the biotic tidal environment with the Zn-SA cathode protection

Table S7 EDS results of the corrosion product on the specimen surface at.%

Position	Fe	O	S	Mg	Ca	Cl	Mn	Na	Zn
1	33.88	61.45	1.75	0.59	0.95	0.26	0.31	0.81	
2	32.68	64.50	2.01	0.19	0.10	0.11	0.07	0.34	
3	32.45	61.98	1.37	0.72	0.57	0.10	0.12	1.69	
4	41.86	53.79	1.21	0.73	0.61	0.12	0.18	1.50	
5	38.73	57.11	1.58	0.86	0.13	0.05	0.68	0.86	
6	57.86	39.49	0.89	0.05	0.06	0.01	1.09	0.55	
7	5.71	61.11	0.82	21.64	0.40	0.85	0.54	3.34	5.57
8	11.06	66.19	0.74	1.67	1.12	0.11	0.08	8.70	10.33
9	48.32	33.61	0.94	0.67	0.22		1.73	7.05	7.46
10	14.28	68.90	0.72	1.79	0.37		0.49	1.53	11.90
11	52.21	26.98	0.82	2.21	1.06	0.27	2.55	2.53	11.37
12	48.68	36.41	0.87	2.49	0.55	0.01	1.09	5.58	4.32
13	10.01	64.53	0.87	3.88	0.72	0.25		10.36	9.38

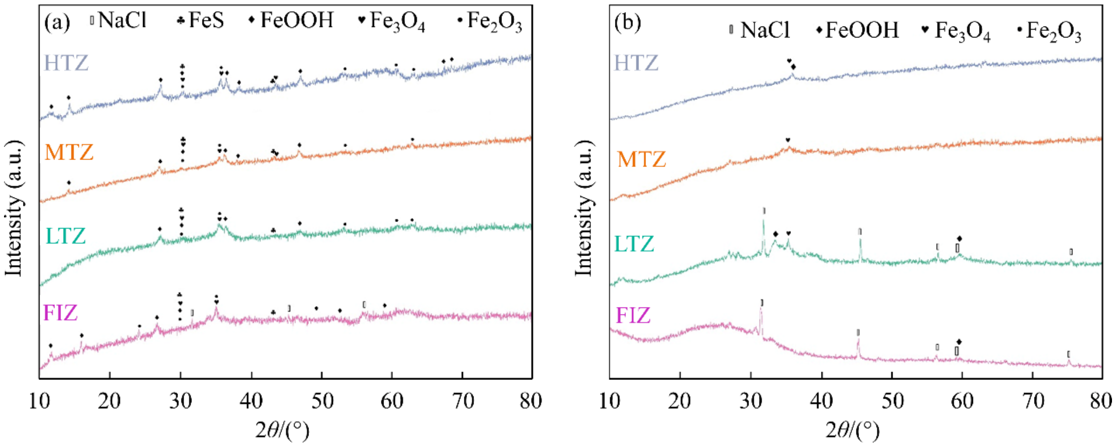

Figure S4 XRD spectra of the corrosion products on the steel surfaces after 360-h exposure in the biotic tidal environments: (a)Without the cathode protection; (b)With the Zn-SA cathode protection

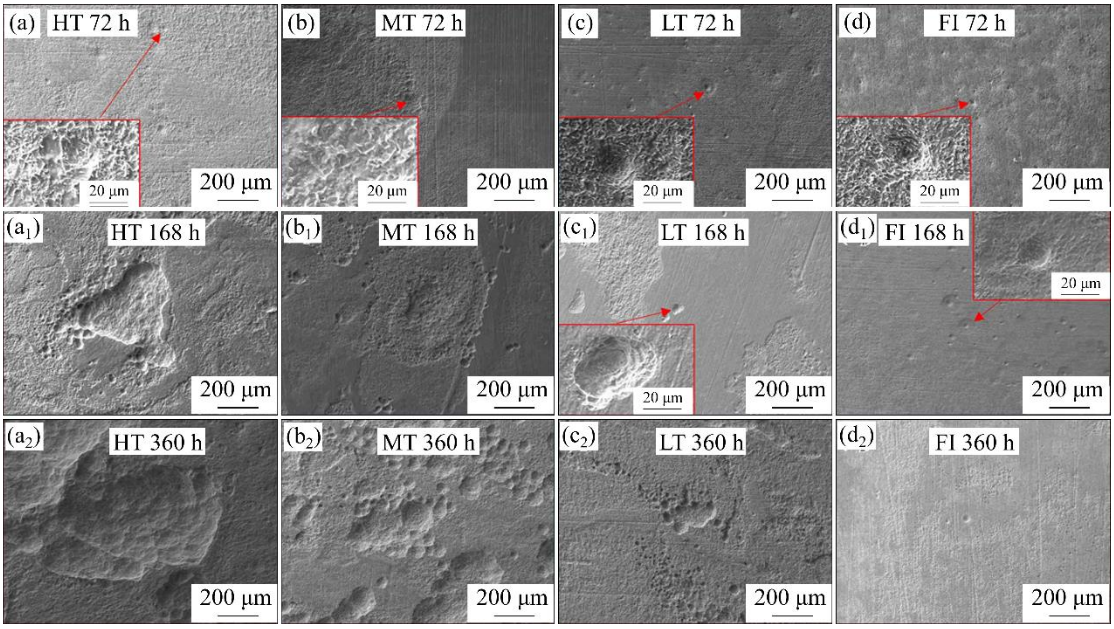

Figure S5 SEM images of the corrosion morphologies of the steel surfaces after 72-h (a–d), 168-h (a_1–d_1) and 360-h (a_2–d_2) exposures in the biotic tidal environment without the cathode

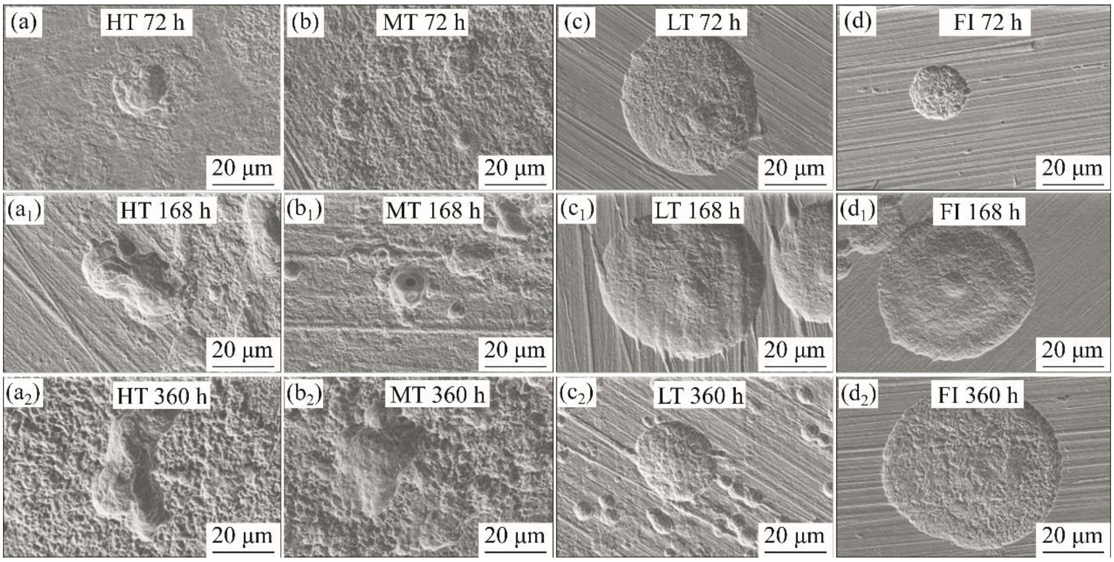

Figure S6 SEM images of the corrosion morphologies of the steel surfaces after 72-h (a–d), 168-h (a_1–d_1) and 360-h (a_2–d_2) exposures in the biotic tidal environment with the Zn-SA cathode protection

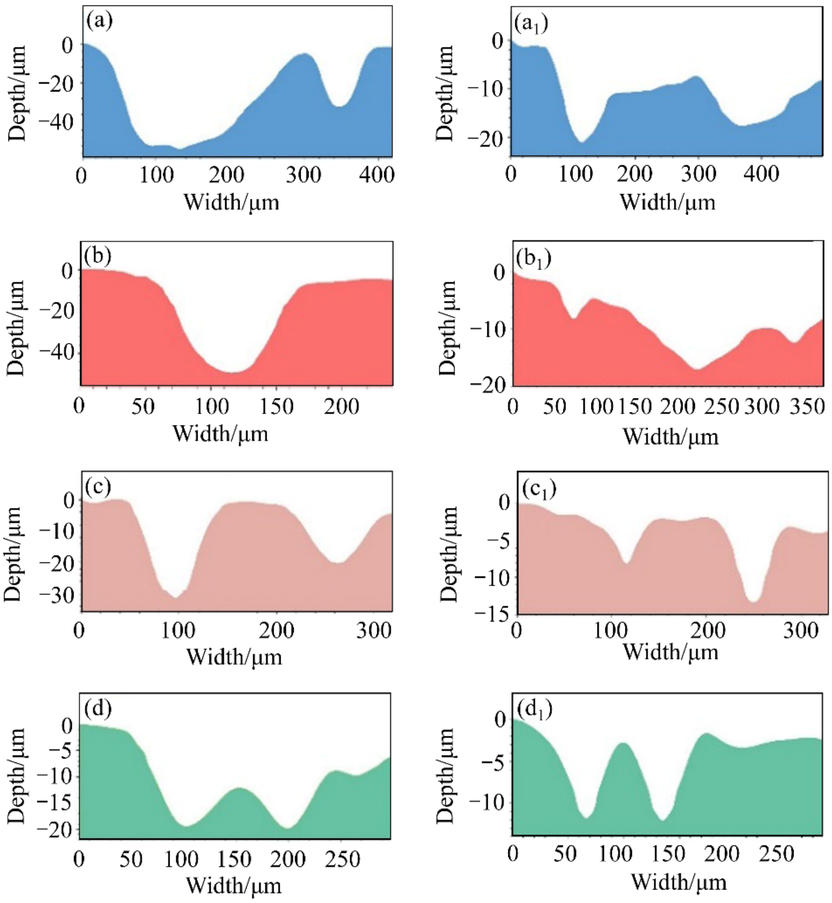

Figure S7 The cross-section of pits on the steel surfaces after 360-h exposure in the biotic tidal environment without cathode protection (a–d) and with Zn-SA cathode protection (a_1–d_1): (a, a_1) HTZ; (b, b_1) MTZ; (c, c_1) LTZ; (d, d_1) FIZ

Table S8 EDS results of the corrosion product on the section morphology at.%

Position	Fe	O	S	Mg	Ca	Cl	Mn	Na	Zn
1	43.61	53.31	1.43	0.15	0.87	0.10		0.52	
2	38.91	59.40	0.04	0.27	0.29	0.12		0.96	
3	18.66	75.50	1.91	0.39	2.44	1.10			
4	47.37	51.57		0.09	0.18	0.26		0.52	
5	23.91	68.33	1.62	5.62	0.24	0.14		0.15	
6	35.42	60.46		3.18	0.45	0.17		0.31	
7	49.35	45.32	2.01		0.30	1.29	1.43	0.30	
8	33.67	62.02	1.12	1.27	0.44	0.83	0.65		
9	40.24	58.17				1.59			
10	26.73	57.49		8.2		1.4			6.18
11	32.27	56.48		6.64	0.84	1.39			2.38
12	20.10	59.14		22.39		3.07			1.50
13	14.34	56.49	0.51	4.39		2.60		7.69	13.97
14	0.88	54.11		3.18	1.05	1.43		16.61	22.74
15	18.83	60.07	0.22	5.16	2.29			6.26	7.17

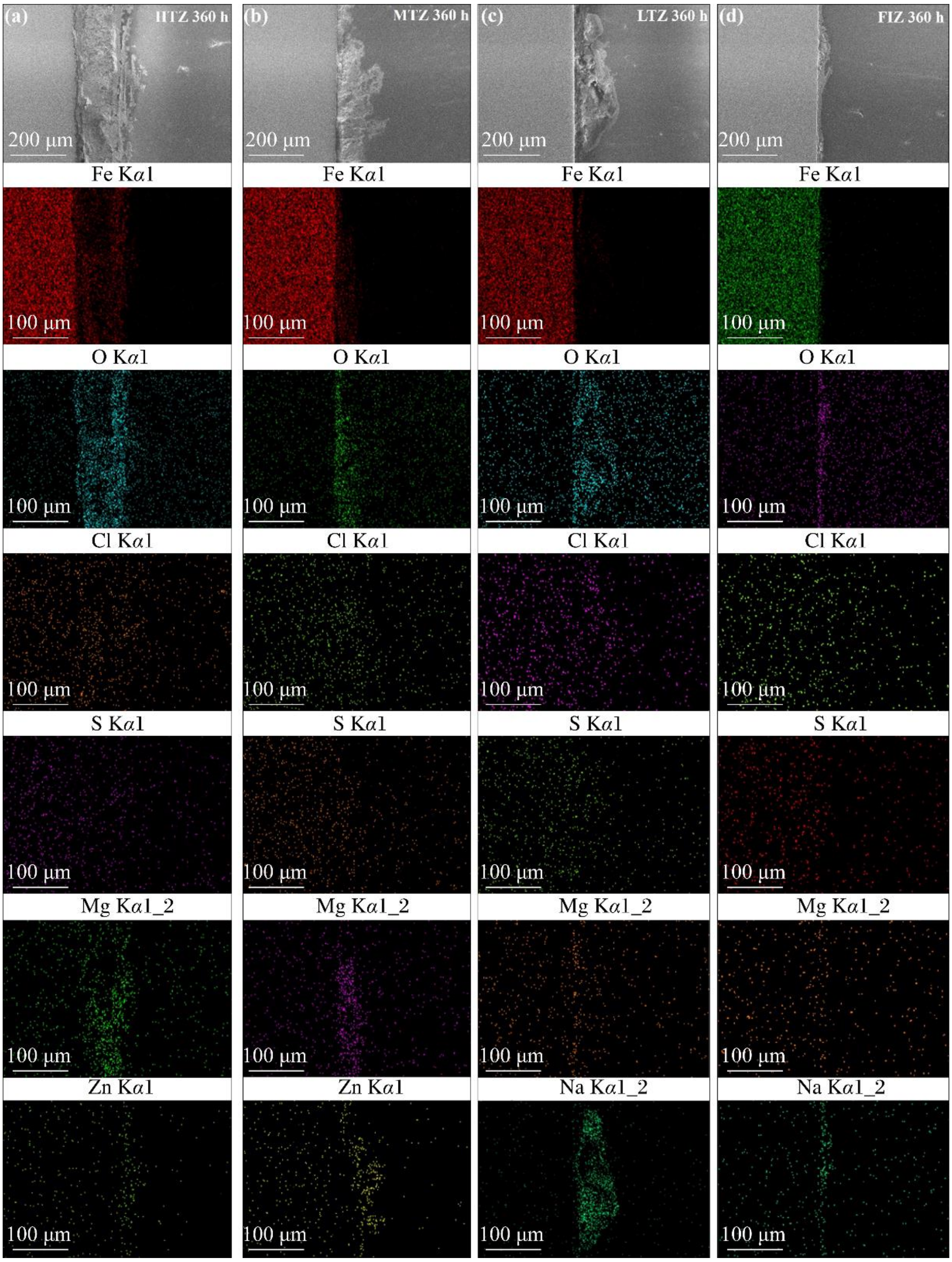

Figure S8 EDS mapping of the cross-section of the steel specimen after 360-h exposure in the biotic marine environment with the Zn-SA cathode protection

Table S9 Fitting results of the polarization curves of the specimens at different zones after 168 h and 360 h tidal cycle in the seawater

Time	Environment	Tidal zone	E_{corr} (vs SCE)/mV	J_{corr}/(μA·cm^{-2})	b_c/(mV·dec^{-1})
168 h	SRB	HTZ	−0.662	49.0	409
		MTZ	−0.670	43.5	409
		LTZ	−0.666	19.1	338
		FIZ	−0.664	4.76	394
	SRB-CP	HTZ	−0.784	6.26	263
		MTZ	−0.781	2.69	275
		LTZ	−0.708	0.836	235
		FIZ	−0.728	0.969	323
360 h	SRB	HTZ	−0.654	76.1	144
		MTZ	−0.654	63.0	448
		LTZ	−0.664	37.3	402
		FIZ	−0.677	4.91	325
	SRB-CP	HTZ	−0.767	5.25	291
		MTZ	−0.713	1.19	255
		LTZ	−0.725	0.522	177
		FIZ	−0.715	0.508	251

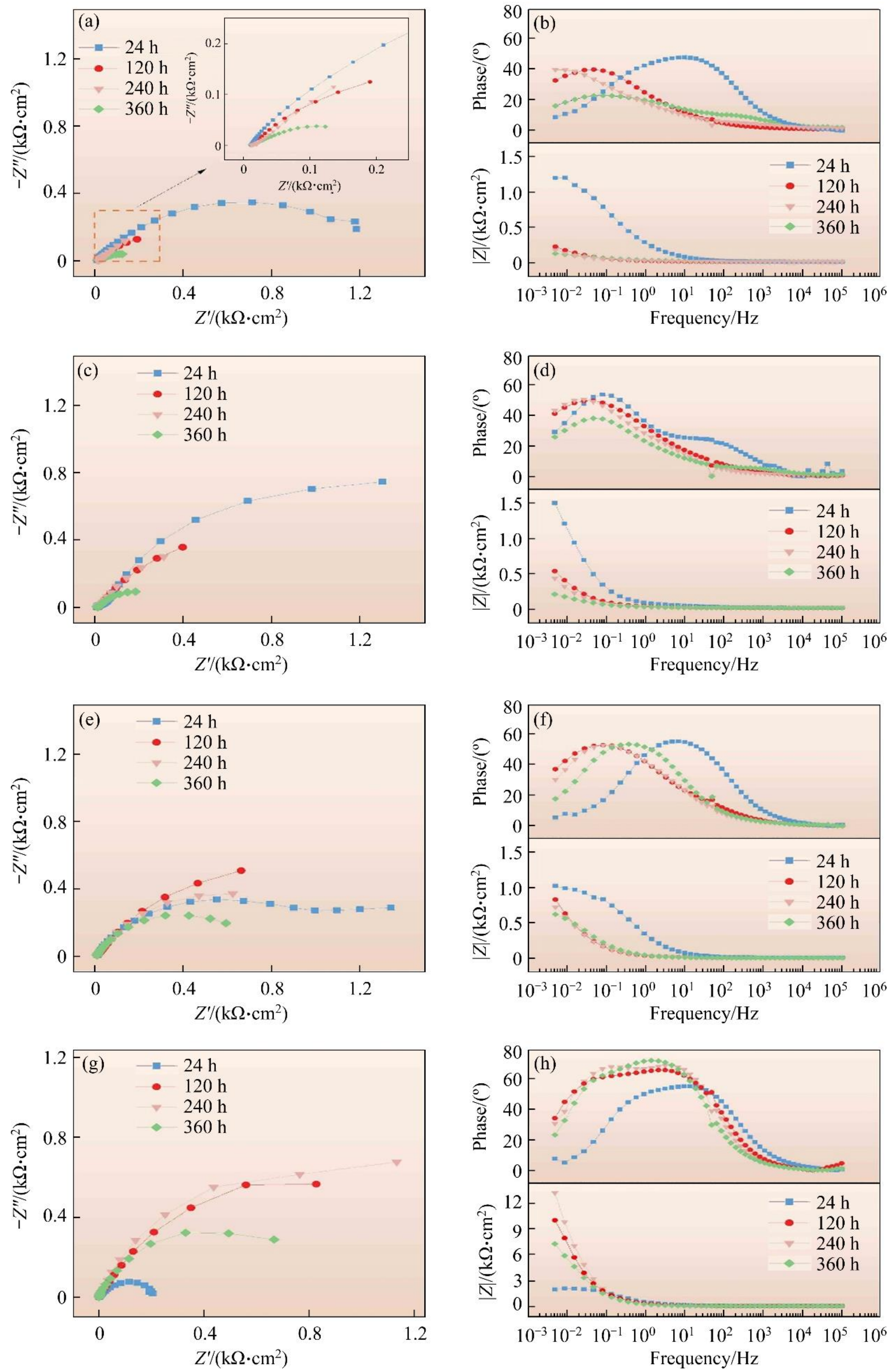

Figure S9 Nyquist plots of the steel during the tidal cycle in the biotic tidal environment without cathode protection: (a, b) HTZ; (c, d) MTZ; (e, f) LTZ; (g, h) FIZ

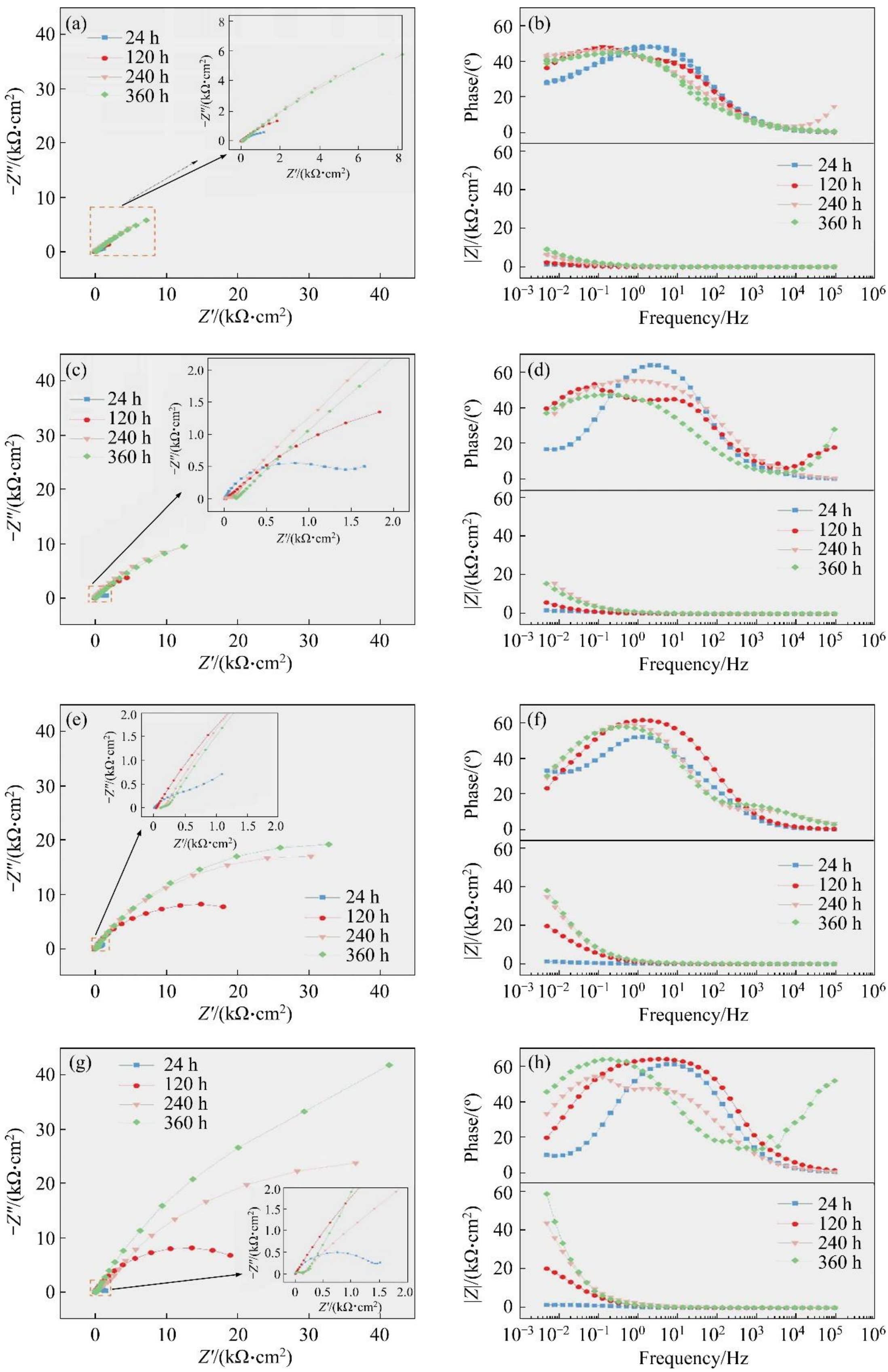

Figure S10 Nyquist plots of the steel during the tidal cycle in the biotic tidal environment with Zn-SA cathode protection: (a, b) HTZ; (c, d) MTZ; (e, f) LTZ; (g, h) FIZ

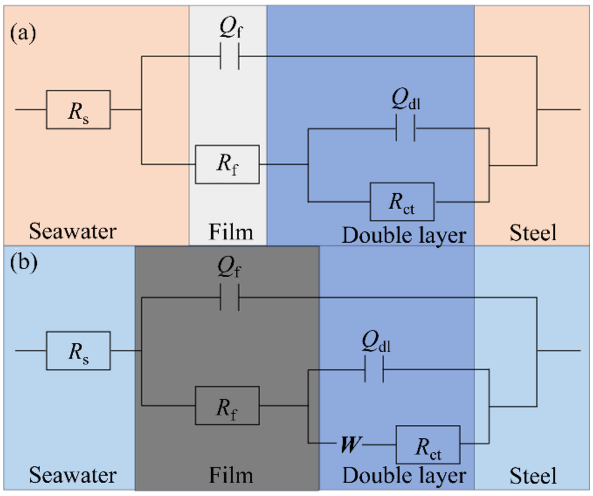

Figure S11 Equivalent circuits for EIS fitting: R_s–solution resistance; Q_f–capacitance of corrosion products film; R_f–resistance of corrosion products film; Q_{dl}–capacitance of electrical double-layer; R_{ct}–charge transfer resistance of electrical double-layer; W–Warburg impedance

Table S10 Fitting results of the EIS data of the steel in HTZ

Environment	Time/h	R_s/(Ω·cm^2)	Y_f/(S·s^n·cm^{-2})	n_f	R_f/(Ω·cm^2)
Without CP	24	11.66	3.104×10^{-4}	0.7892	23.57
	120	11.53	1.560×10^{-2}	0.5444	12.73
	240	11.78	2.001×10^{-2}	0.4425	35.85
	360	11.05	5.022×10^{-3}	0.4806	16.56
With CP	24	10.52	2.171×10^{-3}	0.631	34.19
	120	16.3	1.314×10^{-3}	0.6701	252.2
	240	59.16	7.500×10^{-4}	0.5733	1379
	360	108.8	4.973×10^{-4}	0.5777	1256
Environment	**Y_{dl}/(S·s^n·cm^{-2})**	**n_{dl}**	**R_{ct}/(Ω·cm^2)**	**W/(S·s$^{0.5}$·cm^{-2})**	**χ^2**
Without CP	8.285×10^{-4}	0.4975	1.409		2.627×10^{-4}
	1.050×10^{-2}	0.6531	0.5822		2.700×10^{-4}
	2.403×10^{-2}	0.7386	0.4662		1.721×10^{-4}
	1.755×10^{-2}	0.5166	0.1575		5.248×10^{-4}
With CP	2.385×10^{-5}	0.7463	1.12	7.850×10^{-3}	2.092×10^{-3}
	1.375×10^{-3}	0.7887	1.628	2.796×10^{-3}	6.923×10^{-4}
	1.290×10^{-4}	0.8137	7.618	4.850×10^{-4}	3.908×10^{-3}
	4.442×10^{-5}	0.7154	10.53	4.489×10^{-4}	1.725×10^{-3}

Table S11 Fitting results of the EIS data of the steel in MTZ

Environment	Time/h	R_s/(Ω·cm^2)	Y_f/(S·s^n·cm^{-2})	n_f	R_f/(Ω·cm^2)
Without CP	24	11.49	1.369×10^{-3}	0.6252	61.52
	120	10.93	6.624×10^{-3}	0.6134	16.65
	240	11.97	1.258×10^{-2}	0.6112	53.76
	360	9.845	33.98×10^{-3}	0.5308	6.46
With CP	24	8.506	9.270×10^{-4}	0.7964	208.2
	120	17.89	8.684×10^{-4}	0.6297	1054
	240	36.67	2.327×10^{-4}	0.6975	1681
	360	139.4	2.568×10^{-4}	0.6368	1543
Environment	Y_{dl}/(S·s^n·cm^{-2})	n_{dl}	R_{ct}/(Ω·cm^2)	W/(S·s$^{0.5}$·cm^{-2})	χ^2
Without CP	3.413×10^{-3}	0.8192	1.956		4.688×10^{-3}
	8.097×10^{-3}	0.6838	1.699		3.287×10^{-4}
	9.180×10^{-3}	0.8306	1.424		8.899×10^{-4}
	2.069×10^{-2}	0.6007	0.3887		8.040×10^{-4}
With CP	4.425×10^{-5}	0.6702	1.278	1.212×10^{-2}	8.789×10^{-4}
	5.135×10^{-4}	0.8921	7.747	1.186×10^{-3}	1.479×10^{-2}
	6.637×10^{-5}	0.8285	14.18	3.822×10^{-4}	1.205×10^{-3}
	1.094×10^{-4}	0.71	17.56	4.765×10^{-4}	1.391×10^{-2}

Table S12 Fitting results of the EIS data of the steel in LTZ

Environment	Time/h	R_s/(Ω·cm^2)	Y_f/(S·s^n·cm^{-2})	n_f	R_f/(Ω·cm^2)
Without CP	24	11.59	4.756×10^{-4}	0.7712	26.93
	120	9.662	4.381×10^{-3}	0.6561	19.3
	240	10.49	7.680×10^{-3}	0.6345	67.99
	360	8.668	5.456×10^{-3}	0.689	22.61
With CP	24	10.11	2.306×10^{-3}	0.6605	1132
	120	41.23	2.004×10^{-4}	0.7584	2924
	240	131.9	1.645×10^{-4}	0.7083	11340
	360	155.6	1.451×10^{-4}	0.6894	10890
Environment	Y_{dl}/(S·s^n·cm^{-2})	n_{dl}	R_{ct}/(Ω·cm^2)	W/(S·s$^{0.5}$·cm^{-2})	χ^2
Without CP	2.102×10^{-4}	0.5547	1.002		2.742×10^{-4}
	4.730×10^{-3}	0.7101	1.82		8.805×10^{-5}
	1.458×10^{-3}	0.8728	1.619		9.611×10^{-4}
	7.367×10^{-4}	0.912	0.7601		4.356×10^{-4}
With CP	1.202×10^{-2}	0.7364	1.318	2.822×10^{-2}	6.664×10^{-4}
	5.463×10^{-4}	0.7562	18.22	1.407×10^{-3}	7.942×10^{-4}
	2.160×10^{-6}	0.7849	25.95	3.317×10^{-4}	2.199×10^{-2}
	1.266×10^{-5}	0.8124	28.46	2.901×10^{-4}	3.112×10^{-2}

Table S13 Fitting results of the EIS data of the steel in FIZ

Environment	Time/h	$R_s/(\Omega\cdot cm^2)$	$Y_f/(S\cdot s^n\cdot cm^{-2})$	n_f	$R_f/(\Omega\cdot cm^2)$
Without CP	24	12.11	1.973×10^{-4}	0.8268	69.77
	120	8.232	6.930×10^{-4}	0.8025	2314
	240	8.385	6.499×10^{-4}	0.8449	1849
	360	7.862	9.843×10^{-4}	0.8413	409.6
With CP	24	8.668	5.401×10^{-4}	0.7631	1465
	120	14.7	1.919×10^{-4}	0.7577	4214
	240	155.6	1.183×10^{-4}	0.6418	16080
	360	137.2	1.719×10^{-4}	0.7031	18850
Environment	$Y_{dl}/(S\cdot s^n\cdot cm^{-2})$	n_{dl}	$R_{ct}/(\Omega\cdot cm^2)$	$W/(S\cdot s^{0.5}\cdot cm^{-2})$	χ^2
Without CP	3.360×10^{-4}	0.5981	2.312		1.025×10^{-3}
	3.426×10^{-4}	0.7891	13.89		5.109×10^{-4}
	2.277×10^{-4}	0.8969	15.87		1.615×10^{-3}
	5.217×10^{-5}	0.6584	8.331		1.778×10^{-3}
With CP	6.435×10^{-2}	0.7675	2.466	1.036×10^{-3}	1.642×10^{-5}
	4.832×10^{-5}	0.7416	19.16	4.163×10^{-3}	4.076×10^{-4}
	6.103×10^{-5}	0.9574	54.9	5.194×10^{-4}	2.978×10^{-3}
	6.315×10^{-6}	0.7714	151.9	2.085×10^{-4}	1.421×10^{-1}

S2.1 Macroscopic morphology of corrosion products and corrosion scene

Figure S2 showed the macroscopic morphology of corrosion products and the steels' corroded state after a 360-h exposure to tidal environment without cathode protection. The corrosion products in the FIZ were mainly reddish-brown (Figure S2(d)), while the yellow-brown and/or reddish-brown corrosion products were randomly covered on the steel surface in the marine tidal environment (Figures S2(a)−(c)). After removing the corrosion products (Figures S2(a_1)−(d_1)), areas covered by yellow-brown corrosion products exhibited relatively mild corrosion, contrasting with areas covered by reddish-brown products, which displayed more severe corrosion. Analysis using image Pro Plus 6.0 revealed that areas with substantial corrosion accounted for (93.0±1.1)% in HTZ, (88.4±4.4)% in MTZ, and only (16.7±0.4)% in FIZ (Table S6).

The macroscopic morphology of corrosion products and the steels' corroded condition after 360-h exposure to tidal environment under the Zn-SA cathode protection is showed in Figure S3. In the FIZ, the steel surface exhibited intermittent patches of yellowish-brown corrosion products (Figure S3(d)), while most of the corrosion products in the marine tidal environment were light-yellow, intermixed with white deposits and sporadic reddish-brown corrosion products. Subsequent removal of these corrosion products revealed areas covered by light-yellow corrosion products demonstrating relatively high corrosion levels, while uncovered areas exhibited milder corrosion effects (Figures S3(a_1)−(d_1)). Statistical analysis indicated that under the Zn-SA cathode protection, the proportions of areas experiencing severe corrosion reduced to (75.2±0.9)%, (59.5±9.4)%, (25.0±1.2)% and (10.7±2.2)% in the HTZ, MTZ, LTZ and FIZ, respectively. This was consistent with the corrosion rate findings.

S2.2 XRD results

The XRD patterns of the corrosion products on the steel surfaces after 360-h exposure in the marine tidal environment without and with cathode protection are shown in Figure S4. In the absence of cathode protection, the corrosion products were mainly composed of FeOOH, Fe_2O_3, Fe_3O_4 and FeS. In addition, NaCl was detected in the corrosion products of the specimens from the FIZ. However, under the Zn-SA cathode protection, no obvious peaks of iron oxides in the corrosion products on the steel surface were observed across all tidal zones, suggesting a significant reduction in the iron oxide content within the corrosion products.

S2.3 Corrosion morphology of the steel

The corrosion morphology of the steel in the tidal environments without and with cathode protection, are shown in Figures S5 and S6, respectively. In the absence of cathode protection, there were some small pits on the steel surface across all tidal zones at 72th h, signaling incipient pitting corrosion. Over time, these pits grew in both size and number. The difference in corrosion morphology of the steel gradually increased in different tidal zones. Notably, in the HTZ, the size and number of corrosion pits notably escalated as the experiment progressed. Under the Zn-SA cathode protection, the evolution of corrosion morphology in each tidal zone was similar to that observed without cathode protection. However, the size and number of the corrosion pits significantly decreased under the cathode protection, distinctly indicating the inhibition role of the cathode protection.

References

[1] MU Xin, WEI Jie, DONG Jun-hua, et al. The effect of sacrificial anode on corrosion protection of Q235B steel in simulated tidal zone [J]. Acta Metallurgica Sinica, 2014, 50: 1294−1304.

[2] ZHOU Xiao-bao, WANG Qin, SU Hui, et al. Low efficiency of cathodic protection in marine tidal corrosion of X80 steel in the presence of Pseudomonas sp [J]. Bioelectrochemistry, 2024, 157: 108656. DOI: 10.1016/j.bioelechem.2024.108656.